Published in final edited form as:
J Am Chem Soc. 2008 July 9; 130(27): 8856–8864. doi:10.1021/ja802383t.

Asymmetric Insertion of Membrane Proteins in Lipid Bilayers by Solid-State NMR Paramagnetic Relaxation Enhancement: A Cell-Penetrating Peptide Example

Yongchao Su, **Rajeswari Mani**[†], and **Mei Hong**[*]
Department of Chemistry, Iowa State University, Ames, Iowa 50011

Abstract

A novel solid-state NMR technique for identifying the asymmetric insertion depths of membrane proteins in lipid bilayers is introduced. By applying Mn^{2+} ions on the outer but not the inner leaflet of lipid bilayers, the sidedness of protein residues in the lipid bilayer can be determined through paramagnetic relaxation enhancement (PRE) effects. Protein-free lipid membranes with one-side Mn^{2+}-bound surfaces exhibit significant residual ^{31}P and lipid headgroup ^{13}C intensities, in contrast to two-side Mn^{2+}-bound membranes, where lipid headgroup signals are mostly suppressed. Applying this method to a cell-penetrating peptide, penetratin, we found that at low peptide concentrations, penetratin is distributed in both leaflets of the bilayer, in contrast to the prediction of the electroporation model, which predicts that penetratin binds to only the outer lipid leaflet at low peptide concentrations to cause an electric field that drives subsequent peptide translocation. The invalidation of the electroporation model suggests an alternative mechanism for intracellular import of penetratin, which may involve guanidinium–phosphate complexation between the peptide and the lipids.

Introduction

The depth of protein residues in lipid bilayers is an important aspect of the three-dimensional (3D) structure of membrane proteins. Even before the complete atomic-level high-resolution structure is determined for a membrane protein, knowledge of the depth of its residues already gives information on the topology of the protein in the membrane,[1] which is crucial for understanding its function. Solid-state NMR spectroscopy has provided a number of tools to determine the depth of insertion of membrane proteins. For example, ^{1}H spin diffusion from the lipid chains in the center of the membrane to the protein and from water on the membrane surface to the protein has been exploited.[2–6] Paramagnetic relaxation enhancement (PRE)[7,8] is another powerful approach to measure the site-specific depths of membrane proteins [9–12] or membrane-bound small molecules.[13] Paramagnetic

[*]mhong@iastate.edu.
[†]Present address: Center for Advanced Biotechnology and Medicine, Rutgers, The State University of New Jersey, 679 Hoes Lane, Piscataway New Jersey 08854-5638.

Supporting Information Available: ^{2}H spectra of lipids without and with penetratin. This material is available free of charge via the Internet at http://pubs.acs.org.

ions such as Mn^{2+}, Gd^{3+}, and Dy^{3+} bound to the membrane surfaces enhance the T_2 relaxation rates of nuclear spins in a distance-dependent fashion, so that nuclear spins closer to the membrane surface manifest larger relaxation enhancement, or lower intensities. Membrane-soluble paramagnetic oxygen has also been used to induce depth-dependent changes in chemical shifts and T_1 and T_2 relaxation rates.[14,15] By comparing the protein PRE effects with those of the lipid functional groups whose depths are well-known,[16] one can measure the depths quantitatively.[9] The ability for depth calibration is a unique feature of membrane protein PRE, as compared to PRE applications to macromolecules in solution[17,18] or to microcrystalline proteins.[19]

Despite the many advances in determining membrane protein insertion depths, to our best knowledge there is so far no report of the determination of the asymmetric insertion of membrane proteins in the lipid bilayer. Most membrane proteins insert in a unidirectional fashion as required by their function.[1] It is thus important to determine which leaflet of the bilayer, in addition to the depth, a residue is inserted to. If the paramagnetic ions are distributed on both surfaces of the bilayer, then it is not possible to distinguish the depth in the inner versus the outer leaflet. We demonstrate here a simple modification of the PRE technique that distributes the paramagnetic ions on only one side of the bilayer, thus allowing the determination of the asymmetric insertion depths of membrane proteins. This concept has been shown using lanthanide shift reagents to distinguish outer- and inner-leaflet lipids[20,21] and, in a related approach, to separate extracellular versus intracellular metabolite signals in solution.[22] However, to our best knowledge it has not been applied to membrane peptides and proteins.

We demonstrate the one-side PRE technique on a cell-penetrating peptide (CPP), penetratin. CPPs are Arg- and Lys-rich cationic peptides that have the remarkable ability of transporting macromolecular cargos into cells and the cell nucleus without disrupting the cell membrane.[23–25] As such, CPPs are promising drug-delivery molecules. A large number of biophysical studies have shown that the intracellular import of CPPs is intimately related to their affinity to and interaction with the lipid bilayer.[26] For peptides that directly translocate across the cell membrane, the membrane in question can be the plasma membrane of the cell or, for peptides that enter cells by endocytosis,[27] the endosomal membrane from which the peptides must escape. Given the highly cationic nature of these peptides, their mechanism of translocation across the lipid membrane is intriguing and is the subject of intense study. Penetratin is the first and one of the most extensively studied CPPs and is a 16-residue peptide corresponding to the third helix of the *Drosophilia antennapedia* homeodomain.[28]

Three models have been proposed to explain the membrane translocation of CPPs. In the electroporation model,[29] below a threshold peptide concentration, the peptide binds only to the outer leaflet of the bilayer (Figure 1a), thus creating a trans-membrane electric field that alters the lateral and curvature stresses of the membrane. Above the threshold concentration, electroporation-like permeabilization of the membrane occurs, giving rise to transient membrane defects that allow the peptide to distribute to both leaflets of the bilayer (Figure 1b), thus relieving the curvature stress. Isothermal titration calorimetry experiments indicated that the threshold peptide/lipid molar ratio (P/L) of penetratin was 1:20; moreover an anionic lipid fraction of at least ~50% was found to be necessary for translocation.[29,30]

Recently, ^{1}H solution NMR NOESY spectra of bicelle-bound penetratin showed that the depth of penetratin increases with the peptide concentration,[31] which was interpreted as supporting the electroporation model.

The second model proposes that inverse micelles transiently form in the bilayer to trap the peptide from the outer leaflet and release it to the inner leaflet.[32] This model was primarily based on lipid ^{31}P NMR spectra that showed an isotropic peak indicative of micelles in the presence of the peptide.[33] However, the peptide-free control sample exhibited a similar isotropic peak, suggesting that the micelles result from sample preparation procedures rather than peptide binding. Sonication, extrusion, and extensive freeze–thawing all create small lipid vesicles that have high isotropic mobility, which give rise to an isotropic peak in the ^{31}P spectra. In addition, no hexagonal-phase peak was detected in these ^{31}P spectra, ruling out the hexagonal-phase model.[34]

The third model posits that guanidinium-phosphate complexation neutralizes the Arg residues in CPPs, thus allowing the peptides to cross the membrane without a high free-energy penalty. This model was based on phase transfer experiments on oligoarginines[35] and ^{13}C-^{31}P distance measurements of an Arg-rich antimicrobial peptide.[36] A molecular dynamics simulation of HIV Tat (48–60), another well-studied CPP, showed transient association of the Arg residues with phospholipids in the distal leaflet from the binding side, supporting the guanidinium-phosphate association model for Tat translocation.[37]

In this work, we test the electroporation model for penetratin translocation using the one-side Mn^{2+} PRE method. By placing the Mn^{2+} ions only on the outer surface of the lipid bilayer, we readily distinguish the asymmetric outer-leaflet-only binding from the symmetric double-leaflet binding of peptides. In the first scenario, the outer-surface Mn^{2+} ions will broaden the signals of most peptides and thus cause low intensity in the spectra (Figure 1c). In the second scenario, half of the peptide, those in the inner leaflet, will experience minimal PRE, thus much higher intensities will remain in the spectra (Figure 1d). Below, we first demonstrate the feasibility of one-side Mn^{2+} binding by ^{13}C NMR on peptide-free lipid membrane samples, then apply this method to anionic lipid membranes containing penetratin at low and high *P*/*L* ratios, where the electroporation model predicts a change from asymmetric to symmetric insertion. We show that penetratin is bound to both leaflets of the bilayer at both low and high peptide concentrations, thus indicating that the electroporation model does not apply.

Materials and Methods

Lipids and Peptides

All lipids, including 1-palmitoyl -2-oleoyl-*sn*-glycero-3-phosphatidylcholine (POPC), 1-palmitoyl-2-oleoyl-*sn*-glycero-3-phosphatidylglycerol (POPG), 1,2-dimyristoyl-*sn*-glycero-3-phosphochloline (DMPC), 1,2-dimyristoyl-*sn*-glycero-3-phosphatidylglycerol (DMPG), were purchased from Avanti Polar Lipids (Alabaster, AL) and used without further purification. Penetratin (RQIKI WFQNR RMKWK K) samples incorporating uniformly ^{13}C,^{15}N-labeled residues were synthesized by Fmoc solid-phase protocols and

purified by HPLC to >95% purity.[38] Three peptide samples, containing labeled residues at I3, I5, Q8, N9, and K13, were used in this work.

Membrane Sample Preparation

Oriented membrane samples on glass plates were prepared using a naphthalene-incorporated method as described before.[39,40] Unoriented hydrated liposomes for magic-angle spinning (MAS) experiments were prepared by an aqueous-phase mixing protocol.[38] POPC/POPG membranes with molar ratios of 8:7 or 13:7 were used for all PRE experiments. The mixed lipids were freeze–thawed eight times and extruded through 100 nm pores to produce large unilamellar vesicles (LUVs) of ~100 nm diameter. Peptide-containing samples used peptide/lipid molar ratios (*P*/*L*) of either 1:15 or 1:40. The membrane mixtures were ultracentrifuged above the phase transition temperature to obtain pellets, which were then packed into 4 mm MAS rotors.

Mn^{2+} ions were incorporated into the membrane samples using one of two methods. For pure membrane samples without the peptide, the $MnCl_2$ solution was added to the LUVs after extrusion but before ultracentrifugation (UC). Mn^{2+} ions cannot penetrate the hydrophobic part of the bilayer, which is known from earlier work on Mn^{2+} ions as well as lanthanide ions added to sonicated small unilamellar vesicles.[20] Thus, as long as the bilayers do not reassemble, the Mn^{2+} ions are naturally confined to the outer surface of the bilayers (see Figure 2a). ^{31}P and ^{13}C NMR spectra were used to confirm that UC does not perturb the unilamellar nature of the vesicles and retains the one-sided nature of the Mn^{2+} distribution. To create peptide-containing one-side Mn^{2+} samples, we added the Mn^{2+} solution to the ultracentrifuged membrane pellet. Adding Mn^{2+} ions to the LUV solution before UC was found to lead to two-side Mn^{2+} distribution by ^{31}P NMR, possibly due to transient membrane defects caused by the peptide. In contrast, the dense membrane pellet retains the one-sided nature of the Mn^{2+} distribution, as shown by the ^{31}P spectra and the lipid headgroup ^{13}C MAS intensities (Figure 2c). All Mn^{2+} containing samples used a Mn^{2+} concentration of 8 mol % of lipids.

To create two-side Mn^{2+}-bound membrane samples, after Mn^{2+} binding, the LUVs were freeze–thawed eight times. The freezing process fragments the LUVs by ice formation[41] and thawing reassembles the lipids so that Mn^{2+} ions are now distributed on both sides of each bilayer (Figure 2b).[42] The freeze–thawed vesicles may be oligolamellar rather than unilamellar.

For peptide-lipid ^{13}C–^{31}P REDOR experiments, d_{54}-DMPC/ DMPG (8:7) membrane mixtures were used. The saturated lipids have a higher phase transition temperature of 23 °C, thus better suppressing undesired peptide and lipid motions.

Solid-State NMR Experiments

NMR experiments were carried out on a Bruker AVANCE-600 (14.1 T) and DSX-400 spectrometer (Karlsruhe, Germany). Low temperature was achieved using Kinetics Thermal Systems XR air-jet sample cooler (Stone Ridge, NY) connected to the 400 MHz system. ^{13}C chemical shifts were referenced externally to the ^{13}CO signal of α-glycine at 176.49 ppm on

the tetramethylsilane scale. ^{31}P chemical shifts were referenced to the ^{31}P signal of hydroxyapatite at +2.73 ppm on the phosphoric acid scale.

Direct polarization (DP) and cross polarization (CP) magic-angle spinning (MAS) experiments were conducted with ^{1}H decoupling field strengths of ~62.5 kHz. Typical radiofrequency (rf) pulse lengths were 5 μs for ^{13}C and 4 μs for ^{1}H. All PRE experiments were carried out at 295 K, which is ~25 K above the above the phase transition temperature of the two lipids. 2D ^{13}C–^{13}C correlation experiments were measured at 303 K using the DARR sequence with a mixing time of 30 ms.

Static ^{31}P DP experiments on oriented membrane samples were carried out in a custom-designed 6 mm 12 rectangular The × mm 5 coil. glass plates were × mm inserted into the magnet with the alignment axis parallel to the magnetic field. A typical 5 μs excitation pulse of ^{31}P and a 50 kHz ^{1}H decoupling field were used. Static ^{2}H NMR spectra were measured at 310 K using a quadrupolar echo pulse sequence with a ^{2}H 90° pulse length of 5 μs.

^{13}C{^{31}P} REDOR experiments was conducted on a 4 mm ^{1}H-^{13}C-^{31}P triple-resonance MAS probe using a REDOR pulse sequence with a soft Gaussian π pulse on the ^{13}C channel to remove ^{13}C–^{13}C *J*-coupling.[43,44] To suppress lipid and peptide motions, all REDOR experiments were carried out at 233 K.

Results

One-Side Mn^{2+}-Bound Lipid Membranes

When added to lipid bilayers with negatively charged phosphate groups at the surface, the Mn^{2+} ion is naturally confined to the outer surface and cannot cross the bilayer to the inner surface due to its cationic nature (Figure 2a). Only when the bilayer is disrupted and the lipids reassembled can the phosphate-bound Mn^{2+} ions redistribute to both surfaces of the bilayer. Thus, any processes that cause bilayer reassembly, such as freeze–thaw and sonication, should be avoided when making one-side Mn^{2+}-bound membranes. Conversely, two-side Mn^{2+}-bound lipid membranes can be formed by freeze–thawing the Mn^{2+}-bound lipid vesicles (Figure 2b). For our membrane samples, once the Mn^{2+} solution is mixed with the lipid vesicles, the samples are kept above the phase-transition temperature of the lipids so that the lipid bilayers do not undergo reorganization.

We first verified the one-sided nature of Mn^{2+}-binding on POPC/POPG bilayers without any peptide. Figure 3a shows the ^{31}P static spectra of the lipids before and after Mn^{2+} addition. The Mn^{2+}-bound sample gave a spectrum with 30% of the height of the control sample. Since the sample~ is a pellet obtained after ultracentrifugation, the presence of significant intensity indicates that ultracentrifugation does not disrupt the bilayer.

Figure 3b shows the ^{13}C DP-MAS spectra of the Mn^{2+}-free and one-side Mn^{2+}-bound POPC/POPG bilayers. The site resolution of the ^{13}C MAS spectra and known depths of lipid functional groups allow us to monitor the intensity as a function of depths. The more embedded groups should experience less T_2 relaxation enhancement and thus retain higher intensity. The normalized intensity of each peak, S/S_0 where S corresponds to the Mn^{2+}-

bound sample and S_0 corresponds to the control sample, should exhibit a monotonic increase with increasing depth. To facilitate comparison between different samples, we further normalize the S/S_0 of each peak with the S/S_0 of the chain-end methyl carbon ω. Experiments show that the S/S_0 values for the ω group fall within 80–120% in the DP spectra for the 16- and 18-carbon chain lengths of POPC and POPG lipids. Figure 3c shows the double-normalized intensity, $(S/S_0)/(S/S_0)_\omega$, for all resolved lipid signals. The trend is indeed roughly monotonic. At 8% Mn^{2+}, the headgroup and glycerol signals show dephasing values of 35–45% compared to ω. Importantly, the same sites have vanishing intensities in the two-side Mn^{2+}-bound samples, thus confirming the one-sided nature of the nonfreeze–thawed samples. The headgroup choline Cγ exhibits higher intensity than α and β due to the fast three-site jumps of each methyl group around the Cγ-N axis and the three-site jumps between the methyl groups around the N-Cβ axis. Compared to the headgroup and glycerol carbons, the acyl chain sites from C3 to the chain termini show higher intensities. The largest slope in the curve occurs at the C2–C3 transition. As we have shown before,[9] changing the Mn^{2+} concentration shifts the position of the maximum slope: lower Mn^{2+} concentrations shift the depth-sensitive region toward the surface, while higher Mn^{2+} concentrations shift the depth-sensitive region toward the membrane center.

Predicted PRE Effects of Symmetrically and Asymmetrically Inserted Proteins in Lipid Bilayers

If a membrane peptide is predominantly distributed in the outer leaflet of the membrane, then its intensities should be low in both the one-side and two-side Mn^{2+}-bound samples (Figure 1c). However, if the peptide is symmetrically distributed in both leaflets of the membrane, then the half of the peptide molecules in the inner leaflet should experience minimal PRE from the outer surface, so that the one-side Mn^{2+}-bound sample should have much higher intensity than the two-side Mn^{2+}-bound sample (Figure 1d). Quantitatively, assuming $(S/S_0)_\omega$) 1, then the normalized PRE intensity of each lipid functional group is $0.5(S/S_0)_L + 0.5$ in the one-side Mn^{2+} bound sample, where the constant 0.5 results from the inner leaflet lipids far from the outer-surface Mn^{2+} ions. The intensity decreases to $(S/S_0)_L$ for the two-side Mn^{2+}-bound bilayers, where $(S/S_0)_L \leq 1$. If the peptides are bound only to the outer leaflet, then its PRE intensities are $(S/S_0)_P$ in both the one-side and two-side Mn^{2+}-bound samples. In contrast, if the peptides are distributed in both leaflets symmetrically, then the PRE intensities are $0.5(S/S_0)_P + 0.5$ in the one-side Mn^{2+}-bound sample, which is larger than $(S/S_0)_P$ for the two-side Mn^{2+}-bound sample. Thus, a peptide inserted only in the outer leaflet should have little intensity change between the one-side and two-side Mn^{2+}-bound samples, while a symmetrically bound peptide exhibits intensity decrease from the one-side Mn^{2+}-bound sample to the two-side Mn^{2+}-bound sample.

One-Side and Two-Side Mn^{2+}-Bound Membranes Containing Penetratin

Before applying the one-side Mn^{2+} PRE method to penetratin, we first tested the effect of penetratin binding to the lipid bilayer, to verify that the peptide does not destroy the lamellar structure by forming pores or micelles, which would scramble the Mn^{2+} ions onto both surfaces of the bilayer. Figure 4a,b shows the static ^{31}P spectra of uniaxially aligned POPC/POPG (8:7) membrane and POPC/cholesterol (55:45) membrane without the peptide and with 4 mol % peptide. The membranes are well aligned in the absence of the peptide. The

addition of penetratin increased powder intensities indicative of misalignment but did not create sharp isotropic signals indicative of isotropic phases. Thus, the lamellar morphology of the bilayer is retained in the presence of the peptide.

One-side and two-side Mn^{2+} PRE experiments are carried out at peptide concentrations of *P*/*L*) 1:40 and 1:15, respectively. ^{31}P static spectra confirming the one-sided and two-sided nature of Mn^{2+} binding are shown in Figure 4c. As predicted, once the membrane sample is subjected to freeze–thawing, the ^{31}P intensity is completely destroyed due to lipid reassembly and Mn^{2+} distribution on both bilayer surfaces. Figure 5 shows the ^{13}C DP-MAS spectra of U-I3,N9-labeled penetratin in POPC/POPG (8:7) membranes at four combinations of *P*/*L* ratios and Mn^{2+} sidedness. The Mn^{2+}-bound spectra are superimposed with the Mn^{2+}-free control spectra. For all resolved sites, the double-normalized intensities are plotted in Figure 6. The lipid intensities give the expected monotonic increase with depth, unperturbed by Mn^{2+} binding. In comparison, the penetratin PRE intensities at *P*/*L*) 1:40 cover the range of C2 to the double bond of the acyl chains in the one-side Mn^{2+} sample (Figure 6a). The I3 CR is more shielded from the Mn^{2+} ions than N9 CR, suggesting that the peptide backbone may be tilted relative to the membrane plane. Upon converting the sample to two-side Mn^{2+} by freeze–thaws, the peptide intensities decreased to the range of glycerol G3 to acyl chain C2, indicating closer distances to the surface (Figure 6b). This is consistent with the peptide being distributed in both leaflets of the membrane. Moreover, comparison of the peptide PRE intensities with the lipid intensities shows that the peptide exhibits shallower depths in the one-side Mn^{2+}-bound samples than in the two-side Mn^{2+}-bound samples. For example, the I3 CR PRE corresponds to a depth similar to the lipid C2 and C3 sites for the outer leaflet, but when Mn^{2+} is bound to both bilayer surfaces, the I3 Cα PRE shifts to the lipid G1 to chain C2 (Table 1).

At *P*/*L*) 1:15, the peptide signals also show a general decrease from the one-side Mn^{2+}-sample to the two-side Mn^{2+} sample (Figure 6c,d). Thus, the peptide is similarly embedded in both leaflets of the membrane. In the one-side Mn^{2+}-bound membrane, the peptide has a significant depth distribution between the backbone and the side chain: the overall depth ranges from C2 to the end of the acyl chains, while the backbone CR depth is much more narrowly defined, between ω–1 and the double bond (Figure 6c, Table 1). For the two-side Mn^{2+} sample, the backbone and side chain combined exhibit a depth range from C2 to the middle of the chains, but the backbone lies between the double bond and C3 (Figure 6d). Thus, similar to the low-concentration sample, the peptide backbone has a shallower average depth in the two leaflets than in the outer leaflet alone, indicating that penetratin in the inner leaflets lies closer to the inner surface than those in the outer leaflet do to the outer surface.

^{13}C CP-MAS spectra reproduced the trend of the DP-based PRE curve; however, the CP depth curve is noisier, as a result of the sensitivity of the intensity of highly mobile lipid groups to the ^{1}H–^{13}C CP matching condition. Table 1 summarizes the depths of all measured backbone CR sites, including I3,N9 and K13.

^{13}C–^{31}P Distances between Penetratin and the Lipids

We also measured ^{13}C-^{31}P distances between penetratin and the lipid phosphate groups to determine the quantitative depth of the peptide from the membrane surface without

distinguishing the sidedness. To freeze the peptide and lipid motions, the experiments were carried out at 233 K, well into the gel phase of the DMPC/DMPG membrane. Figure 7 shows the REDOR decay curves of the labeled residues. The distances fall in the range of 6.9 – 8.2 Å, with the N-terminal residues having slightly longer distances than the C-terminal residues (Table 2), in good agreement with the PRE results obtained from the LC phase of the bilayer. We simulated the REDOR curves assuming two-spin systems. As we showed recently, the incorporation of multiple ^{31}P spins into the simulation only lengthens the individual ^{13}C–^{31}P distances, but the actual vertical distance from the ^{13}C to the ^{31}P plane is slightly shorter than the apparent two-spin distance. For example, a REDOR curve that corresponds to a two-spin distance of 8.0 Å, when simulated assuming a five-spin system, gives a vertical ^{13}C–^{31}P plane distance of ~7.0 Å.[36] A two-spin distance of 7 Å corresponds to a vertical distance of 5.2 Å in a five-spin simulation. Here, we use only the ~ two-spin distances in considering the relative depths of individual residues from the membrane surface.

Discussion

Penetratin Insertion Does Not Proceed by Electroporation

Comparison of the one-side and two-side Mn^{2+} PRE data clearly indicates that penetratin is inserted into both leaflets of the anionic lipid bilayer even at the low *P*/*L* ratio of 1:40, which is well within the concentration regime previously considered to have asymmetric binding.[29] The fact that the one-side Mn^{2+} samples have high peptide intensities is possible only if (1) the peptide is deeply embedded in the outer leaflet alone, (2) if half of the molecules are embedded in the inner leaflet and experience minimal PRE while the other half of the molecules are inserted in the outer leaflet, or (3) if all the peptides are solely distributed in the inner leaflet. Scenario 3 can be ruled out because it would require higher peptide PRE intensities than even the membrane-center ω group, which is inconsistent with the experimental observation. Scenario 1 is also ruled out since distributing Mn^{2+} ions to both surfaces of the bilayer caused intensity reduction in the ^{13}C spectra. Therefore, in the *P*/*L* regimes of 1:40–1:15, penetratin is inserted into both leaflets of the lipid bilayer. This result disproves the electroporation model for penetratin.[29]

Figure 8 summarizes the depth information obtained from the PRE data in the liquid-crystalline phase, supplemented by the REDOR data from the gel-phase membrane. Penetratin is distributed in both leaflets of the bilayer, with an average depth closer to the inner surface than the outer surface. At *P*/*L*) 1:40, the peptide is located near the upper part of the acyl chains, with the backbone slightly tilted with respect to the membrane surface so that the N-terminus is more buried than the C-terminus. At *P*/*L*) 1:15, the peptide backbone is more deeply buried and near the middle of the acyl chains (Table 1).

We represent the peptide schematically with a turn-rich conformation with no α-helical or β-sheet structures. This information was obtained from extensive ^{13}C chemical shift and dipolar coupling data:[38] the peptide conformation falls into the “random coil” regime in the liquid-crystalline phase of the membrane. However, the Cα and Cβ C–H order parameters are 0.23–0.52 instead of 0, and chemical shift anisotropies are uniaxially averaged, indicating that the peptide undergoes anisotropic, uniaxial motion around the bilayer normal.

Thus, we hypothesized that the peptide adopts a turn conformation, which would satisfy both the secondary chemical shift constraints and the dynamics data. The significance of this conformation may be that it minimizes the hydrophobic interaction between the peptide and the lipid chains, which would facilitate passage of the peptide through the bilayer and into the cell.

While the PRE data rule out asymmetric insertion at peptide concentrations of *P*/*L*) 1:40 and higher, it does not rule out the possibility that at much lower concentrations the peptide may still be asymmetrically inserted. However, we think this scenario is unlikely as an equilibrium state of the peptide, since at *P*/*L*) 1:40 the average peptide depth is already shifted toward the inner surface of the membrane.

Smith and co-workers used ^{1}H NOESY experiments to characterize the depth of insertion of penetratin in DMPC/ DMPG/DHPC(10:3:13)bicelles.[31] Byobservingthelipid–peptide cross peaks in the 2D NOESY spectra, they found that the peptide contact with the lipid chains increased with the peptide concentration. This concentration dependence of cross-peak intensity was interpreted as supporting the electroporation model. However, the ^{1}H NOESY technique, like most NMR techniques, does not distinguish the two sides of the lipid bilayer. Our current data is consistent with the Smith report in that penetratin shows an increased depth in each leaflet as the peptide concentration increases (Figure 6). However, the two-sided nature of penetratin binding is already present at the low *P*/*L* and remains unchanged at the high *P*/*L*. Thus, the most essential feature of the electroporation model, the asymmetric binding, is invalid within the concentration regimes examined here.

The Mn^{2+} PRE data shown here indicate that penetratin side chains adopt somewhat different depths from the backbone. For example, at *P*/*L*) 1:15, the side chains show clearly lower intensities than the backbone, indicating closer proximity to the membrane surface. This suggests that there may exist possible interactions between the side chains and the membrane surface phosphate groups, an example of which has been shown recently in a cationic antimicrobial peptide.[36]

^{2}H NMR spectra (Figure S1, Supporting Information) of chain-perdeuterated d_{54}-DMPC/ DMPG bilayers show very similar quadrupolar couplings in the absence and presence of penetratin. This is consistent with the aligned bicelle ^{2}H spectra[31] and indicates that penetratin does not perturb the order of the hydrophobic core of the membrane significantly.

Since neither the inverse micelle model nor the electroporation model are consistent with solid-state NMR data, what mechanism explains the translocation of penetratin through lipid membranes? Combining the high-temperature conformation, dynamics, and depth of the peptide[38] we have determined, we propose the following model. Initially penetratin binds to the membrane through electrostatic attraction, then the concentration gradient of the peptide from the extracellular space to the membrane drives insertion into the membrane. Once in contact with the membrane, the compact turn-shaped molecule has minimal hydrophobic interaction with the lipid chains that retains it in the membrane. Moreover the cationic Arg and Lys side chains preferentially interact with the lipid phosphate groups in the distal

membrane leaflet.[36,37] These two factors drive penetratin to cross the lipid bilayer rapidly into the intracellular solution.

Application of the Asymmetric PRE Technique for Studying Membrane Protein Topology

The one-side Mn^{2+} PRE approach for lipid bilayers is generally applicable. Most membrane proteins insert into lipid bilayers with a unique orientation and topology;[1] thus, the site-specific insertion depths are an important component of structure determination. Various extensions of the outer-leaflet Mn^{2+}-PRE technique can be envisioned: for example, inner-leaflet Mn^{2+} PRE is possible with suitable treatment of the lipid vesicles,[45] and covalent linkage of Mn^{2+} ions to membrane proteins may also be feasible, similar to what has been shown for DNA–protein complexes in solution.[17,18] In addition to membrane protein topology, functionally important membrane asymmetry between the two leaflets[46] can be readily investigated with this technique by detecting suitable lipid signals. Although we demonstrated this one-side PRE approach using only 1D ^{13}C experiments due to the good resolution of the mobile and site-specifically labeled penetratin, 2D and 3D experiments can be employed when needed to obtain high resolution for larger membrane proteins. The experiment is also not restricted to only the lipid chain-end ω peak for normalizing the PRE intensities; thus, direct ^{13}C excitation is not mandatory. The large $(CH_2)_n$ peak of the lipid, for example, has reproducible CP intensities; thus, for lipids of the same chain lengths, the $(CH_2)_n$ signal can serve as an intensity reference with a known average depth. As an example, Figure 9 shows the 2D ^{13}C–^{13}C DARR[47] correlation spectra of a control and a two-side Mn^{2+}-bound sample of POPC/POPG membranes containing I3,N9-labeled penetratin. The dephasing of the cross peaks are readily measured, and the separation of the peptide cross peaks from the lipid background ^{13}C signals along the diagonal is a significant advantage of the 2D spectroscopy. For Figure 9, the cross peak S/S_0 of the peptide peaks is normalized with respect to the S/S_0 of the lipid ω–1 peak at 23.5 ppm along the diagonal. The cross peak dephasing values reflect the average depths between the two carbons establishing the cross peak. Since the two carbons are spatially close, the average depth does not compromise the depth information.

Supplementary Material

Refer to Web version on PubMed Central for supplementary material.

Acknowledgments

We thank Professor Alan Waring (UCLA) for providing the (I3,N9)-labeled peptide sample. This work is funded by an NIH Grant GM-066976 to M.H.

References

1. von Heijne G. Nat. Rev. Mol. Cell Biol. 2006; 7:909–918. [PubMed: 17139331]
2. Kumashiro KK, Schmidt-Rohr K, Murphy OJ, Ouellette KL, Cramer WA, Thompson LK. J. Am. Chem. Soc. 1998; 120:5043–5051.
3. Huster D, Yao XL, Hong M. J. Am. Chem. Soc. 2002; 124:874–883. [PubMed: 11817963]
4. Luo W, Hong M. Solid State NMR. 2006; 29:163–169.

5. Etzkorn M, Martell S, Andronesi OC, Seidel K, Engelhard M, Baldus M. Angew. Chem., Int. Ed. 2007; 46:459–462.
6. Hong M. J. Phys. Chem. B. 2007; 111:10340–10351. [PubMed: 17685648]
7. Bloembergen N. J. Chem. Phys. 1957; 27:572–573.
8. Solomon I. Phys. Rev. 1955; 99:559–565.
9. Buffy JJ, Hong T, Yamaguchi S, Waring A, Lehrer RI, Hong M. Biophys. J. 2003; 85:2363–2373. [PubMed: 14507700]
10. Tuzi S, Hasegawa J, Kawaminami R, Naito A, Saito H. Biophys. J. 2001; 81:425–434. [PubMed: 11423425]
11. Grobner G, Glaubitz C, Watts A. J. Magn. Reson. 1999; 141:335–9. [PubMed: 10579957]
12. Prosser RS, Evanics F, Kitevski JL, Patel S. Biochim. Biophys. Acta. 2007; 1768:3044–3051. [PubMed: 17976526]
13. Villalain J. Eur. J. Biochem. 1996; 241:586–93. [PubMed: 8917460]
14. Prosser RS, Luchette PA, Westerman PW. Proc. Natl. Acad. Sci. U.S.A. 2000; 97:9967–9971. [PubMed: 10954744]
15. Luchette PA, Prosser RS, Sanders CR. J. Am. Chem. Soc. 2002; 124:1778–1781. [PubMed: 11853456]
16. Wiener MC, White SH. Biophys. J. 1992; 61:434–447. [PubMed: 1547331]
17. Iwahara J, Clore GM. Nature. 2006; 440:1227–1230. [PubMed: 16642002]
18. Iwahara J, Anderson DE, Murphy EC, Clore GM. J. Am. Chem. Soc. 2003; 125:6634–6635. [PubMed: 12769564]
19. Nadaud PS, Helmus JJ, Höfer N, Jaroniec CP. J. Am. Chem. Soc. 2007; 129:7502–7503. [PubMed: 17530852]
20. Nolden PW, Ackermann T. Biophys. Chem. 1976; 4:297–304. [PubMed: 985701]
21. Kumar VV, Malewicz B, Baumann WJ. Biophys. J. 1989; 55:789–792. [PubMed: 2720071]
22. Aime S, Botta M, Mainero V, Terreno E. Magn. Reson. Med. 2002; 47:10–13. [PubMed: 11754437]
23. Eguchi A, Akuta T, Okuyama H, Senda T, Yokoi H, Inokuchi H, Fujita S, Hayakawa T, Takeda K, Hasegawa M, Nakanishi M. J. Biol. Chem. 2001; 276:26204–26210. [PubMed: 11346640]
24. Gratton JP, Yu J, Griffith JW, Babbitt RW, Scotland RS, Hickey R, Giordano FJ, Sessa WC. Nat. Med. 2003; 9:357–362. [PubMed: 12598894]
25. Schwarze SR, Ho A, Vocero-Akbani A, Dowdy SF. Science. 1999; 285:1569–1572. [PubMed: 10477521]
26. Fischer R, Fotin-Mleczek M, Hufnagel H, Brock R. ChemBioChem. 2005; 6:2126–2142. [PubMed: 16254940]
27. Richard JP, Melikov K, Vives E, Ramos C, Verbeure B, Gait MJ, Chernomordik LV, Lebleu B. J. Biol. Chem. 2003; 278:585–590. [PubMed: 12411431]
28. Derossi D, Joliot AH, Chassaing G, Prochiantz A. J. Biol. Chem. 1994; 269:10444–10450. [PubMed: 8144628]
29. Binder H, Lindblom G. Biophys. J. 2003; 85:982–995. [PubMed: 12885645]
30. Drin G, Cottin S, Blanc E, Rees AR, Temsamani J. J. Biol. Chem. 2003; 278:31192–31201. [PubMed: 12783857]
31. Zhang W, Smith SO. Biochemistry. 2005; 44:10110–10118. [PubMed: 16042388]
32. Derossi D, Calvet S, Trembleau A, Brunissen A, Chassaing G, Prochiantz A. J. Biol. Chem. 1996; 271:18188–18193. [PubMed: 8663410]
33. Berlose JP, Convert O, Derossi D, Brunissen A, Chassaing G. Eur. J. Biochem. 1996; 242:372–386. [PubMed: 8973656]
34. Prochiantz A. Curr. Opin. Neurobiol. 1996; 6:629–634. [PubMed: 8937827]
35. Rothbard JB, Jessop TC, Lewis RS, Murray BA, Wender PA. J. Am. Chem. Soc. 2004; 126:9506–9507. [PubMed: 15291531]
36. Tang M, Waring AJ, Hong M. J. Am. Chem. Soc. 2007; 129:11438–11446. [PubMed: 17705480]

37. Herce HD, Garcia AE. Proc. Natl. Acad. Sci. U.S.A. 2007; 104:20805–20810. [PubMed: 18093956]
38. Su Y, Mani R, Doherty T, Waring AJ, Hong M. J. Mol. Biol. in press.
39. Hallock KJ, Henzler Wildman K, Lee DK, Ramamoorthy A. Biophys. J. 2002; 82:2499–2503. [PubMed: 11964237]
40. Mani R, Buffy JJ, Waring AJ, Lehrer RI, Hong M. Biochemistry. 2004; 43:13839–13848. [PubMed: 15504046]
41. Traikia M, Warschawski DE, Recouvreur M, Cartaud J, Devaux PF. Eur. Biophys. J. 2000; 29:184–195. [PubMed: 10968210]
42. Mayer LD, Hope MJ, Cullis PR, Janoff AS. Biochim. Biophys. Acta. 1985; 817:193–196. [PubMed: 4005257]
43. Jaroniec CP, Tounge BA, Rienstra CM, Herzfeld J, Griffin RG. J. Am. Chem. Soc. 1999; 121:10237–10238.
44. Jaroniec CP, Tounge BA, Herzfeld J, Griffin RG. J. Am. Chem. Soc. 2001; 123:3507–3519. [PubMed: 11472123]
45. Oku N, MacDonald RC. Biochemistry. 1983; 22:855–863. [PubMed: 6682337]
46. Daleke DL. J. Lipid Res. 2003; 44:233–242. [PubMed: 12576505]
47. Takegoshi K, Nakamura S, Terao T. Chem. Phys. Lett. 2001; 344:631–637.

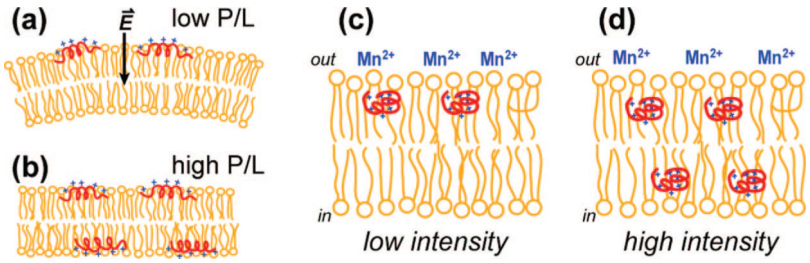

Figure 1.

One-side paramagnetic relaxation enhancement NMR for determining the asymmetric binding of membrane proteins. (a, b) Electroporation model of cell-penetrating peptides. (a) At low *P*/*L*, the peptides are bound to the outer leaflet of the membrane, causing an electric field and membrane curvature strain. (b) At high *P*/*L*, the peptides distribute to both leaflets of the membrane, releasing the curvature strain. When Mn^{2+} ions are distributed on the outer surface of the membrane: (c) Membrane proteins inserted only to the outer leaflet experience strong PRE and give low intensities. (d) Membrane proteins bound to both leaflets of the bilayer have high intensities due to the negligible PRE experienced by the inner-leaflet molecules.

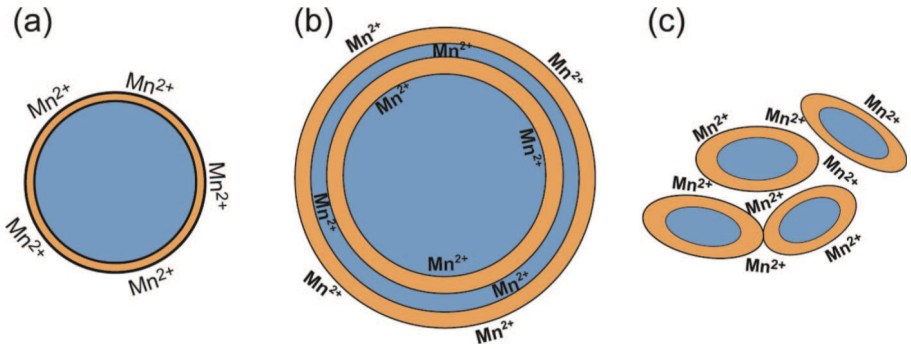

Figure 2.

One-side and two-side Mn^{2+}-bound membrane samples. Orange: lipids. Blue: water. (a) One-side Mn^{2+}-bound large unilamellar vesicles before ultracentrifugation. Mn^{2+} ions are distributed only on the outer surface of the bilayer. (b) Two-side Mn^{2+}-bound membranes after freeze-thawing. Oligolamellar vesicles form where Mn^{2+} ions are distributed on both sides of each bilayer. (c) Mn^{2+} ions added to the membrane pellet after ultracentrifugation. The Mn^{2+} ions diffuse between unilamellar vesicles and remain on the outer surface of the bilayers.

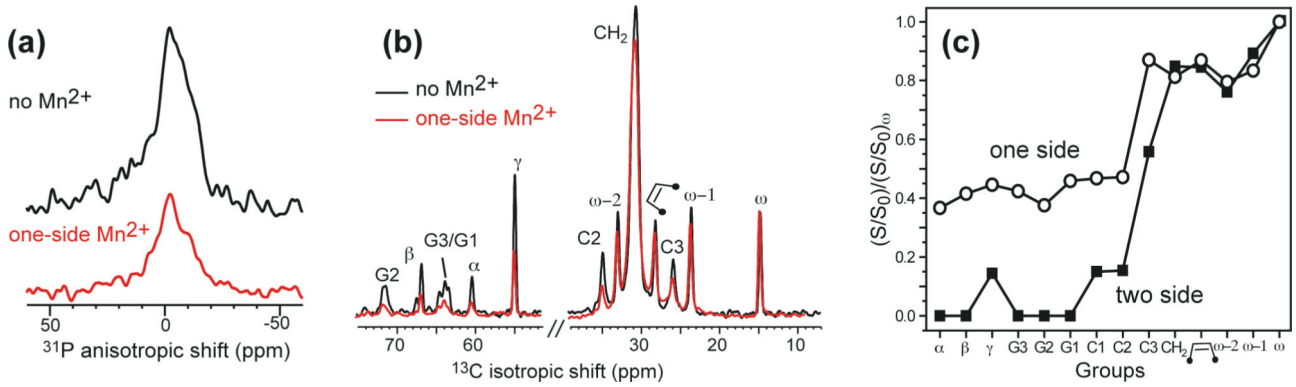

Figure 3.

^{31}P static and ^{13}C MAS spectra of POPC/POPG (3:1) vesicles without any peptide. (a) ^{31}P static spectra without Mn^{2+} (top) and with Mn^{2+} on one-side (bottom). (b) ^{13}C MAS spectra without Mn^{2+} (black) and with (red) one-side Mn^{2+}. (c) Double-normalized intensity of Mn^{2+}-bound POPC/POPG membranes. (○) One-side Mn^{2+}-bound membrane. (■) Two-side Mn^{2+}-bound membrane.

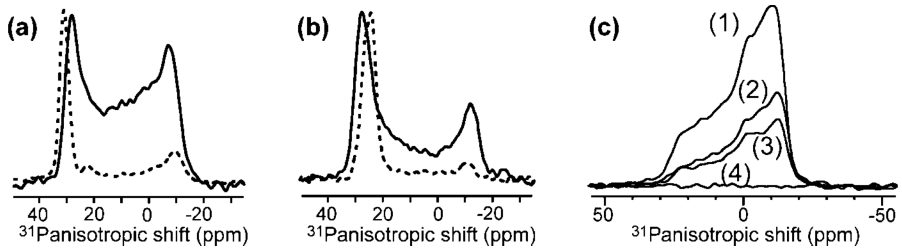

Figure 4.

Static ^{31}P spectra of lipid membranes showing the effects of penetratin on membrane disorder and of Mn^{2+} on ^{31}P intensity. (a) Oriented ^{31}P spectra of POPC/POPG (8:7) bilayers without (dashed line) and with 4 mol % penetratin (solid line). (b) Oriented ^{31}P spectra of POPC/cholesterol (55:45) bilayers without (dashed line) and with 4 mol % penetratin (solid line). The lipid membranes are oriented on thin glass plates. Note the absence of any isotropic peak. (c) ^{31}P powder spectra of penetratin-containing POPC/POPG (8:7) membrane before and after the addition of Mn^{2+}. Compared to the full control spectrum without Mn^{2+} (1), 15 min after addition of Mn^{2+} a roughly 2-fold intensity reduction is seen (2). Three days after Mn^{2+} addition the ^{31}P intensity is largely retained (3), indicating that rf pulses do not cause Mn^{2+} scrambling. After freeze–thawing the membrane the ^{31}P intensity is completely suppressed by the strong PRE effect (4).

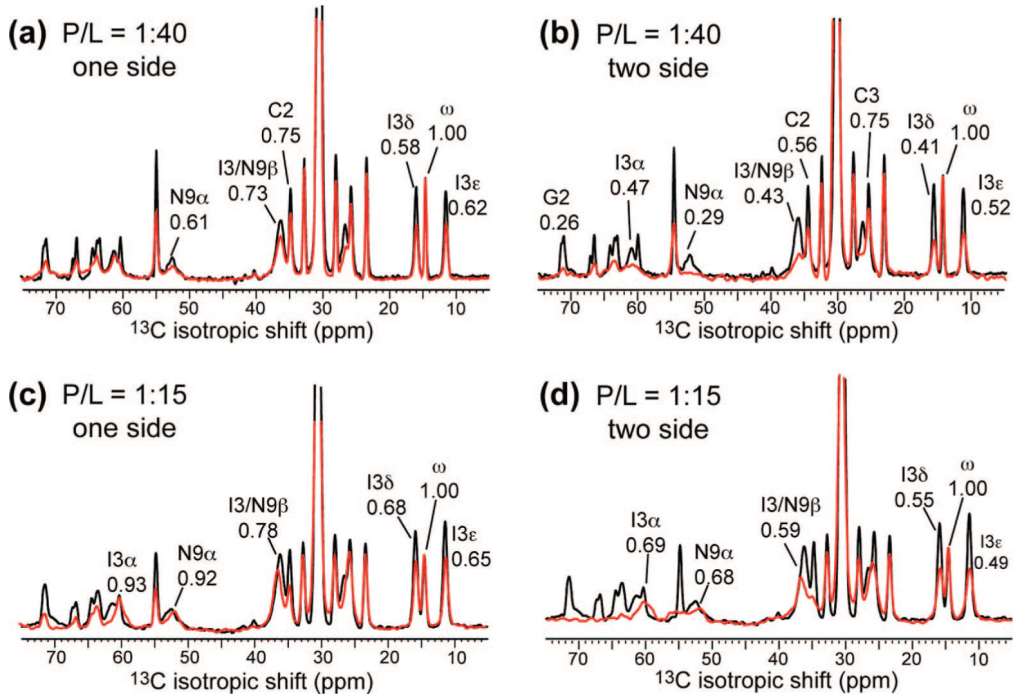

Figure 5.

^{13}C DP-MAS spectra of I3,N9-labeled penetratin in POPC/POPG (8:7) membranes under different peptide concentrations and Mn^{2+} binding methods. (Red) Mn^{2+}-bound spectra. (Black) Mn^{2+}-free control spectra. (a) *P*/*L*) 1:40, with one-side Mn^{2+}. (b) *P*/*L*) 1:40, with two-side Mn^{2+}. (c) *P*/*L*) 1:15, with one-side Mn^{2+}. (d) *P*/*L*) 1:15, with two-side Mn^{2+}. Assignments are shown for key peptide and lipid peaks.

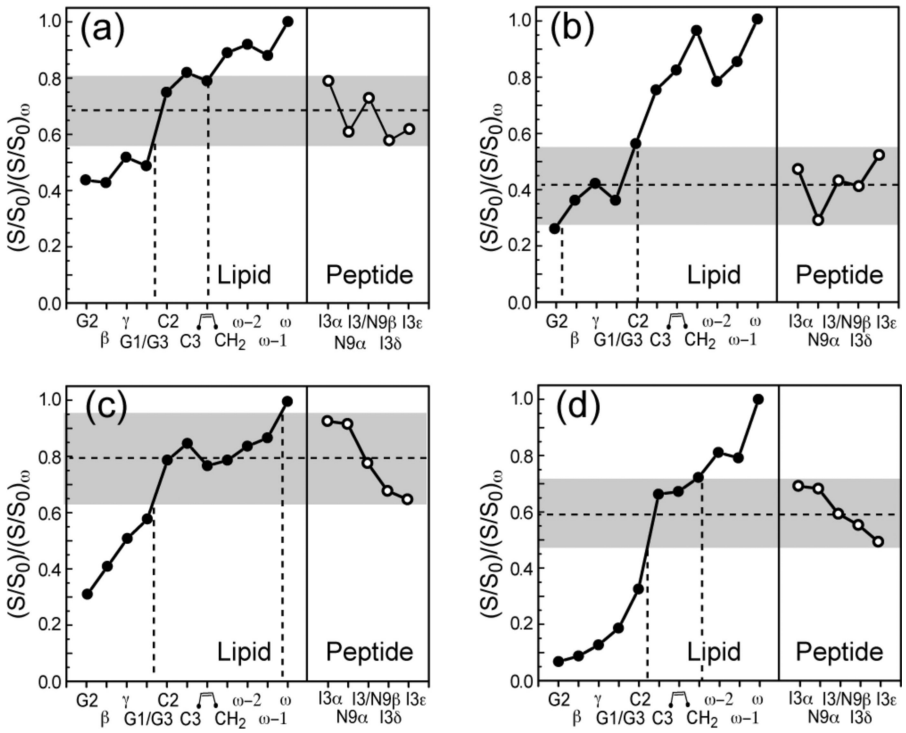

Figure 6.

Normalized intensities of penetratin in POPC/POPG (8:7) bilayers at 295 K. (a) *P*/*L*) 1:40, with one-side Mn^{2+}. (b) *P*/*L*) 1:40, with two-side Mn^{2+}. (c) *P*/*L*) 1:15, with one-side Mn^{2+}. (d) *P*/*L*) 1:15, with two-side Mn^{2+}.

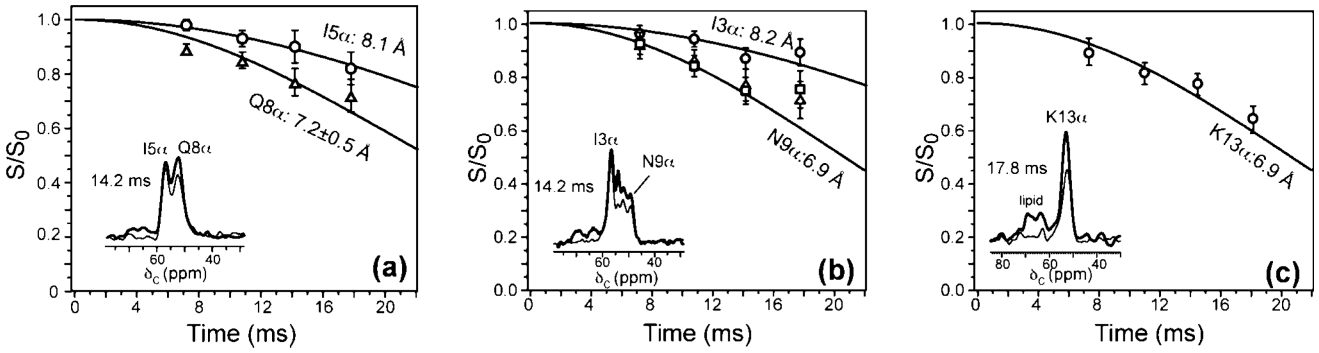

Figure 7.

^{13}C–^{31}P REDOR curves of penetratin in DMPC/DMPG bilayers at 233 K and *P*/*L*) 1:15. (a) I5α and Q8α. (b) I3α and N9α. (c) K13α.

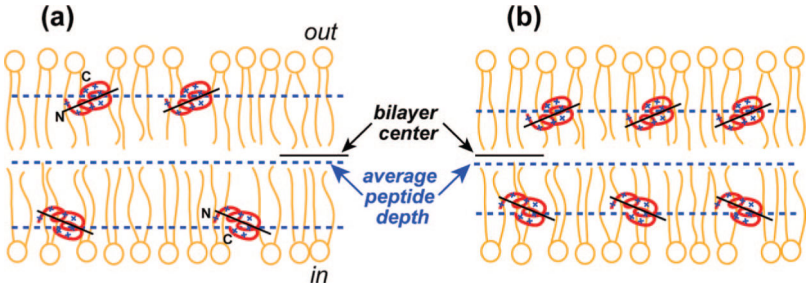

Figure 8.

Symmetry and depth of insertion of penetratin in the anionic POPC/POPG membranes. (a) *P*/*L*) = 1:40. (b) *P*/*L*) = 1:15. In (b) the peptides are more deeply inserted in each leaflet than in (a). However, the common aspects are that the peptide is inserted into both leaflets of the bilayer, the average depth is closer to the inner surface than the outer surface, and the peptide is slightly tilted with respect to the bilayer plane.

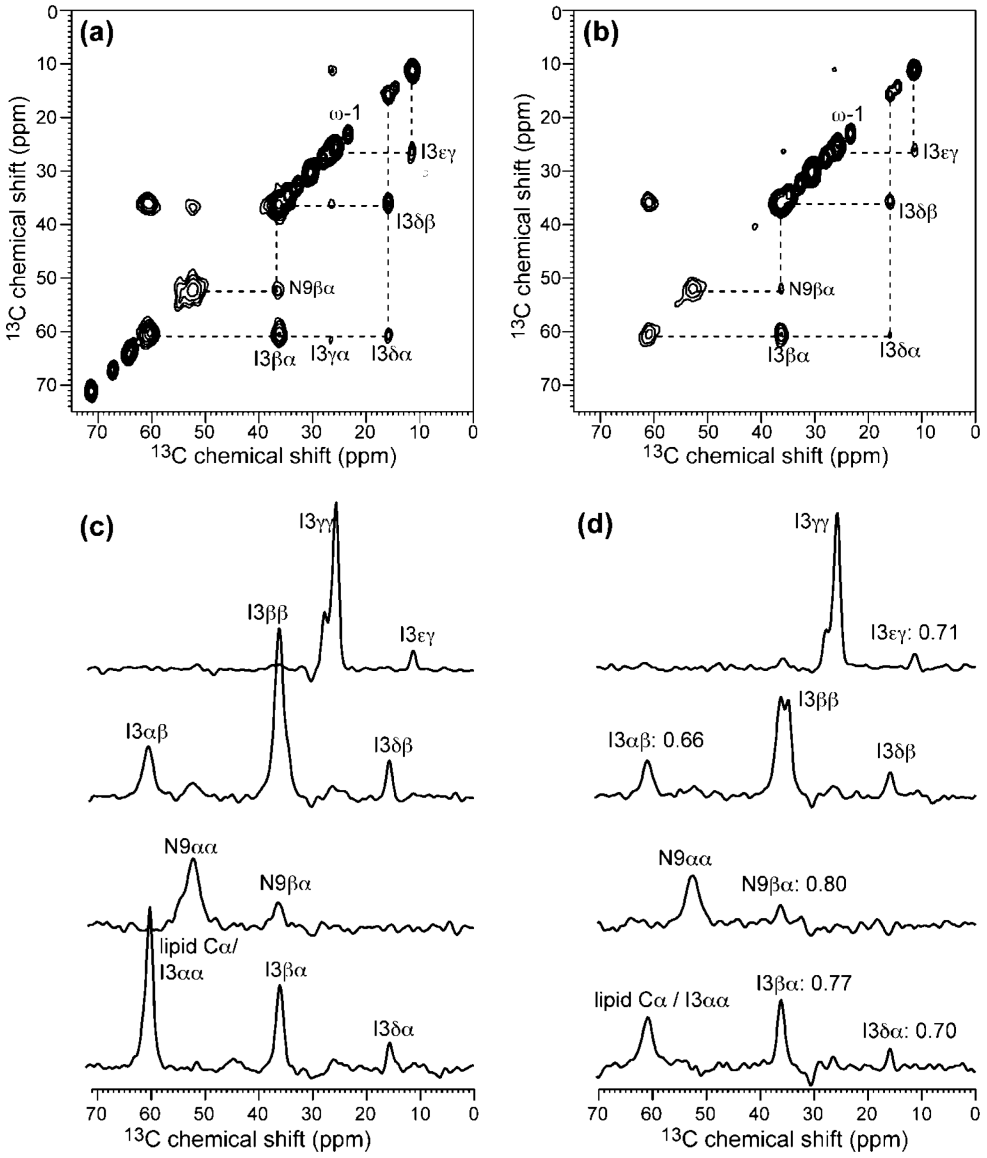

Figure 9.

Two-dimensional ^{13}C–^{13}C correlation spectra of POPC/POPG membranes containing I3,N9-labeled penetratin. (a) Without Mn^{2+}. *P*/*L*) = 1:15. (b) With 8% Mn^{2+} on both sides of the membrane. *P*/*L*) = 1:20. (c, d) Row cross sections at positions indicated by dashed lines in the 2D spectra. (c) Cross sections from (a) give the S_0 intensity. (d) Cross sections from (b) give the *S* intensity. The double normalized intensities $(S/S_0)/(S/S_0)_{\omega\text{-}1}$ of several cross peaks are indicated. The spectra were collected at 303 K under 5.0 kHz MAS using a 30 ms DARR mixing time.

Table 1

Depths of Penetratin Backbone Sites in POPC/POPG (8:7) Membranes from One-Side and Two-Side Mn^{2+} PRE

P/L	site	Mn^{2+} on outer leaflet	Mn^{2+} on both leaflets
1:40	I3 Cα	C2–C3	G1–C2
	N9 Cα	G1–C2	G3
	K13 Cα	C2 –C3	C3–(CH2)n
1:15	I3 Cα	*ω*– 1–*ω*	C9
	N9 Cα	*ω* – *1* – *ω*	C9
	K13 Cα	double bond	C3

Table 2

^{13}C–^{31}P Distances of Penetratin Residues in DMPC/ DMPG (8:7) Membranes at *P/L* = 1:15 and 233 K

residue	I3 Cα	I5 Cα	Q8 Cα	N9 Cα	K13 Cα
distance (A)	8.2	8.1	7.2	6.9	6.9